FEM approach for diagnosis of induction machines' non-adjacent broken rotor bars by short-time Fourier transform spectrogram

Panagiotou, P., Arvanitakis, I., Lophitis, N., Antonino-Daviu, J. A. & Gyftakis, K. N

DOI 10.1049/joe.2018.8240
ESSN 2051-3305

Publisher: IET

The Journal of Engineering

The 9th International Conference on Power Electronics, Machines and Drives (PEMD 2018)

IET Journals
The Institution of Engineering and Technology

FEM approach for diagnosis of induction machines' non-adjacent broken rotor bars by short-time Fourier transform spectrogram

eISSN 2051-3305
Received on 26th June 2018
Accepted on 2nd August 2018
E-First on 14th May 2019
doi: 10.1049/joe.2018.8240
www.ietdl.org

Panagiotis A. Panagiotou[1] ✉, Ioannis Arvanitakis[1], Neophytos Lophitis[1], Jose A. Antonino-Daviu[2], Konstantinos N. Gyftakis[1]

[1]*School of CEM and Research Centre for Mobility & Transport, Coventry University, Coventry, UK*
[2]*Department of Electrical Engineering, Universitat Politècnica de València, Valencia, Spain*
✉ *E-mail: panagio4@uni.coventry.ac.uk*

Abstract: Rotor electrical faults are an issue frequently encountered when applying condition monitoring and fault diagnosis on induction machines. The detection via the analysis of the stator current becomes challenging when the rotor cage suffers from multiple breakages at non-adjacent positions. In that case, electromagnetic asymmetries induced by the broken bars can be masked in such a way, that the diagnostic ability is highly likely to be obscured, thus leading to misinterpretation of the monitored signals' signatures. A new approach is proposed in this work to overcome this problem while the motor is at steady state. In this study, an industrial 6.6 kV, 1.1 MW induction motor is simulated with finite element analysis (FEM) and its electromagnetic variables are analysed and studied under healthy state and several faulty conditions. The analysis of the stator current and stray flux waveforms is executed in both the transient and the steady state and aims to diagnose the challenging cases where the rotor breakages are non-consecutive with regard to their spatial location. The results show the potential of flux analysis to fault severity regardless of the spatial position of the broken bars.

1 Introduction

Although broken rotor bars do not always lead to direct failure of the induction machine, they can cause severe damage after long-term operation in industrial environments or EV applications, where motors undergo excessive load cycles [1–7]. In addition, highly likely to be followed by a double breakage and/or broken end ring, broken bars are frequently compromised with misdiagnosis. This statement is encountered in the majority of past and recent works on this matter, which also outline the broken bar effects and asymmetries in the spectra of stator or rotor current, flux and other electromagnetic characteristics of the motor [1].

One of the typical cases where misdiagnosis during a condition monitoring process becomes likely is at the presence of broken bars or end ring breakages at non-adjacent positions [2]. In this case, depending on the distance between the broken bars, the broken bar fault signatures might be masked in the stator current spectrum and overlooked, resulting in wrong evaluation of indicators for fault symptoms, thus leading to false negative diagnosis [3].

Furthermore, the rapid evolution of variable speed drives demands the monitoring of motors under transient state. Various techniques have been proposed to this direction, analysing signals during transient and steady state in the time-frequency domain. The aim of these techniques is to obtain information from the signal's spectral energy density distribution about where the harmonic trajectories lie regarding frequency and, at the same time, when the transitions of these frequencies happen in time. Among them short-time Fourier transform (STFT) is one of the most frequently used, due to its simplicity in terms of low computational complexity [4–6, 8] and availability in commercial software packages.

Many works on the matter of broken bars outline the significance of non-adjacency and attempt to assess the broken bar fault severity [9, 10]. In [2], the authors provide a detailed analysis of these effects and provide significant evaluation of the broken bar harmonics during the steady state for a two-pole squirrel cage induction machine. Furthermore, the authors of [3] use the STFT to evaluate the amplitudes of high-order harmonics related with double bar faults, while the same time-frequency representation is used in [4] for fault identification in a permanent magnet AC drive.

Moreover, a reliable analysis based on non-conventional broken bar fault indicators is given in [5] using motor current signature analysis (MCSA) and zero-sequence current methods, while in [6] the STFT is used for bearing and lubrication fault detection. A presentation of different time-frequency techniques for fault identification and diagnosis is given in [7] and a comparison of such techniques in [11]. Finally, the STFT is implemented in [8] for achieving a sensorless speed measurement of induction machines and most importantly in [12], where the authors provide significant information about stray flux monitoring after supply disconnection. However, the majority of these works focus on the implementation of spectral estimation or time-frequency techniques during the transient state only. The phenomena that alter the behaviour of the machine during transient – where the FFT method fails to provide accurate information even on healthy machines – also appear on the steady state. In this case, the time-varying behaviour that is likely to be caused by the broken bar fault – and can be indicated by the corresponding time responses of the signals – are likely to appear in the spectral content with the help of a time-frequency method. It is important to note that in many industrial applications, the induction motors work uninterrupted at steady state for long periods. In such cases, the methods based on the starting transient are obviously not easily applicable.

In this paper, a 6.6 kV, 50 Hz, 1.1 MW, 6-poles cage induction motor will be analysed and studied under healthy and faulty conditions. The focus will be given to the reliable identification of non-adjacent rotor breakages, since in those cases traditionally applied steady-state methods like MCSA might fail.

The paper is structured as follows: In Section 2, the induction motor models under investigation with finite element analysis (FEM) are described in detail along with the transform used for the monitored signals' analysis. In Section 2.1, the FEM models are presented and explained, while Section 2.2 provides a brief description of the STFT and the related spectrogram. Section 3 focuses on the analysis of representative results regarding the broken bar fault and how it can be detected through current and flux monitoring. Finally, in Section 4 the conclusions are drawn, while the ongoing and future works are outlined.

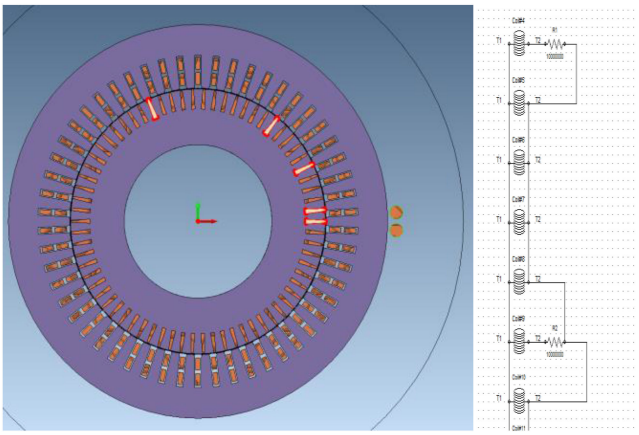

a b

Fig. 1 *FEM modelling*
(a) Cross section of the induction motor FEM model with the positions of the different breakage cases highlighted and, ***(b)*** Part of the rotor circuit with bar 1 and bar 6 being broken

2 FEM modelling and STFT spectrogram

2.1 Description of the motors

For this study, a 6-pole, 6.6 kV, 1.1 MW, 50 Hz cage induction motor with the rotor cage fabricated from copper has been simulated by using the MagNet software from Infolytica. The FEM model takes into account the exact geometrical and materials characteristics which have been provided by the manufacturer. Five distinct cases have been simulated and studied; firstly, the healthy motor is analysed, followed by four different cases accounting for different rotor cage breakages: a case of two adjacent broken bars and three cases of non-adjacent broken bars.

To account for broken rotor bars with FEM, a certain conductivity should be attributed to the broken bar area in order to account for eddy and cross-currents, thus not being an open circuit. Nevertheless, this approach is realistic for motors with cast aluminium rotors, where the rotor bars are not isolated from the iron core, and inter-bar currents are free to circulate. Usually, it is cast aluminium rotors that have skewed bars which further enhance the inter-bar currents. These have an adverse impact on the diagnosis of broken rotor bars because they allow the current flow through the iron, hence negatively influence the fault severity estimation. Despite that, in the case of the motor under investigation, the rotor copper bars are isolated from the iron and they are un-skewed, so no significant inter-bar currents exist. The rotor consist of 70 copper bars and the stator of 54 slots with 12-turn slots per stator phase and double layer winding, while the bodies of both the stator and rotor are made of steel. The active length of the machine is 1152 mm.

The cross section of the studied motor is shown in Fig. 1*a*. Moreover, the highlighted bars on the rotor point the location of the induced breakages. Finally, the magnetic flux sensing coil is observed to the right of the motor's stator. The flux sensor consists of 50 turns and is placed externally from the machine's housing, where the area is accounted for exterior air at room temperature (20°C). Furthermore, Fig. 1*b* depicts the equivalent circuit for one of the non-adjacent broken bar cases. In order to account for a bar breakage in 2D FEM modelling, a resistance of high value is connected in series with the bar coil, since the breakage is desired to be imitated as close as possible with an open circuit.

In Fig. 2, the magnetic field distribution is shown for the healthy motor case. The six magnetic poles of the machine can be seen clearly with uniform symmetry of the magnetic flux lines. On the other hand, the spatial asymmetry of the magnetic field for the different faulty cases is shown in Fig. 3. To aid the reader, the different studied cases are named as follows: Case I: healthy, Case II: two adjacent broken bars, Case III: two non-adjacent broken bars with distance half-pole pitch, Case IV: two non-adjacent broken rotor bars with distance one pole pitch and Case V: two non-adjacent broken rotor bars with distance 2 pole's pitch. This is also shown in Table 1.

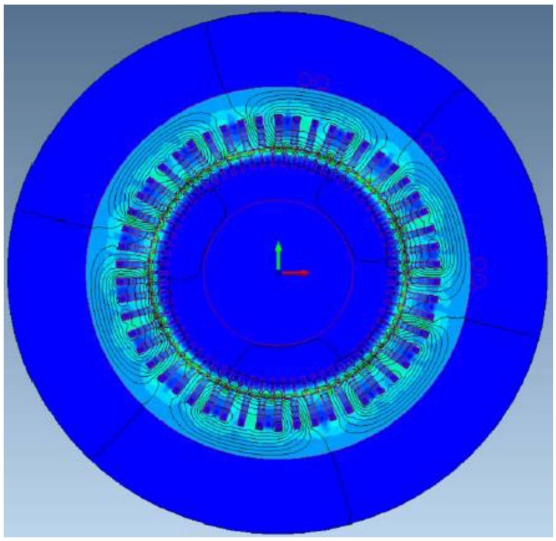

Fig. 2 *Magnetic field distribution for the healthy motor model (Case I)*

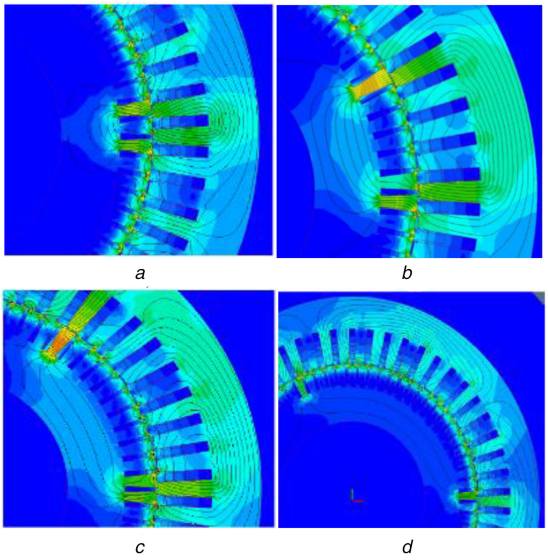

a b c d

Fig. 3 *Motors under simulation and analysis*
(a) Case II, ***(b)*** Case III, ***(c)*** Case IV and ***(d)*** Case V

Table 1 Case studies

Case	Broken bars	Location
II	1 & 2	adjacent
III	1 & 6	within half pole's pitch
IV	1 & 11	within one pole's pitch
V	1 & 23	within two pole's pitch

Starting with Case II (Fig. 3*a*), one can observe the concentrated asymmetry in the magnetic field due to the adjacent bars breakage. However, in the Cases III–V, the breakages inflict local magnetic field asymmetries at two different spatial areas.

2.2 STFT analysis and results

The windowed Fourier transform, most frequently encountered as STFT, offers a time-frequency representation of a signal in terms of providing a picture of the signals' spectral characteristics over time. The visualisation of the frequencies' spectral energy density is provided by the spectrogram. The idea behind the spectrogram is to yield a contour plot of the magnitude, color coded in a scale to express the intensity of the signal's spectral energy magnitude [5, 11, 13].

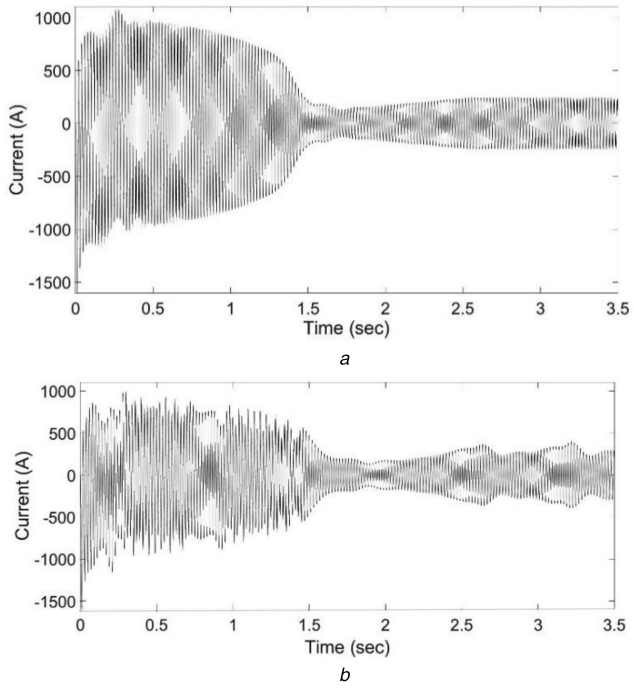

Fig. 4 *Stator current versus time for*
(a) Healthy motor and, ***(b)*** Motor with non-adjacent breakages by one pole pitch

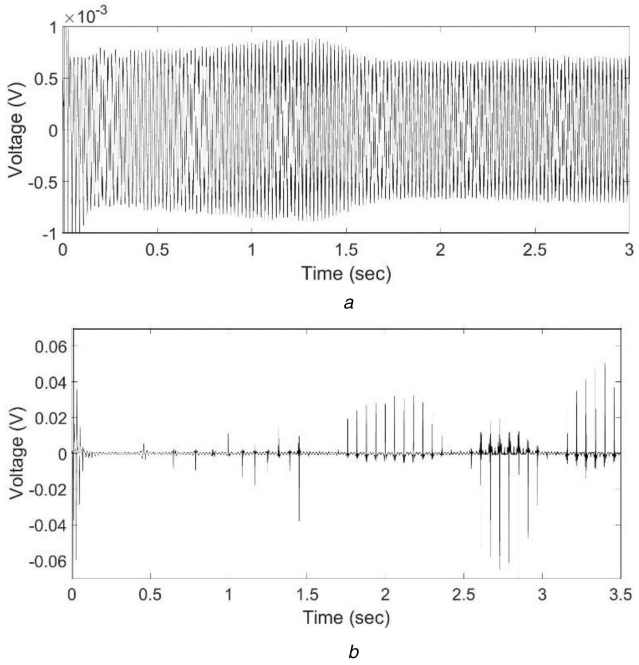

Fig. 5 *Flux sensor voltage versus time for*
(a) Healthy motor and, ***(b)*** Motor with non-adjacent breakages by one pole pitch

The continuous time STFT $X(t, f)$ of a signal is a function of both time t and frequency f – as opposed to FFT that is a function of frequency only – that can be computed from the FFT over a sliding window by the following equation [14]:

$$X(t, f) = \int_{-\infty}^{+\infty} x(t)w(t-\tau)\mathrm{e}^{-j2\pi ft}\mathrm{d}t, \quad (1)$$

where $x(t)$ is the signal of our interest, $w(t)$ is the sliding window, τ is the window shifting factor and $f = 2\pi/\omega$ the frequency. Equation (1) provides a joint time-frequency representation by means of the spectrogram $S(t, f) = |X(t, f)|^2$.

Nevertheless, among the papers dealing with STFT and other time-frequency approaches [15], only a few handle the condition

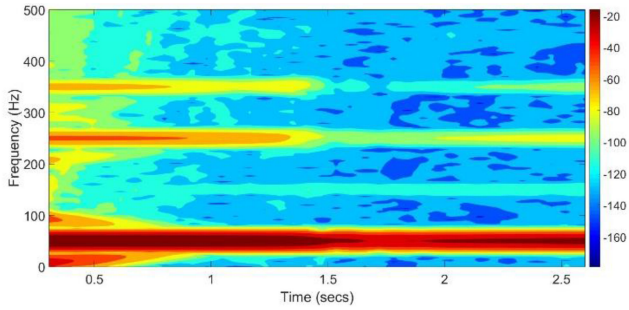

Fig. 6 *Stator current STFT spectrogram of healthy motor*

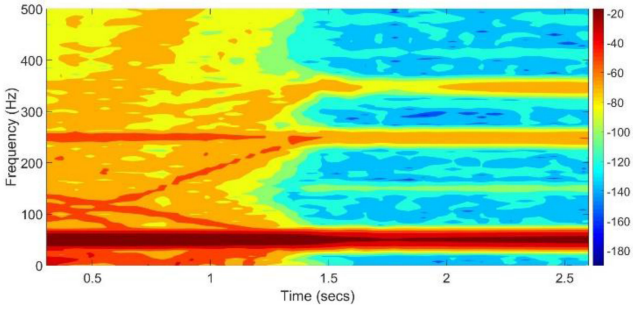

Fig. 7 *Stator current STFT spectrogram of motor with adjacent broken bars (Case II)*

monitoring of electrical machines through the spectrogram of non-current measurements like stray flux and air-gap torque [8, 12].

For the analysis of the studied signals, the discrete time STFT is implemented [14]. A Kaiser window is selected as the sliding window function with $\beta = 150$, of length $L = 2048$ and 90% overlap between the time-frames. This ad-hoc selection of parameters showed a good trade-off between time and frequency resolution, in order to observe the signals' harmonic trajectories in the spectrogram [6, 7].

3 Representative results

In Figs. 4*a* and *b*, the stator current over time is depicted for the healthy motor and one of the motors with non-adjacent broken bars (Case III). It is clear that the transient lasts slightly longer for the faulty motor and that the amplitude oscillation becomes time varying in the steady state.

Furthermore, Figs. 5*a* and *b*, illustrate the flux sensor voltage over time for the healthy motor and for one of the non-adjacent cases of broken bars (Case IV). The faulty motor's signal presents a periodical behaviour with respect to the fault, with local maxima appearing as spikes obeying to the periodicity, hence making their presence every 1.5 s and for a duration of approximately 1 s (Fig. 5*b*).

In Figs. 6 and 7, the spectrograms of stator current for the healthy motor and for the motor with adjacent broken bars are depicted, respectively, during transient and steady state from 0 s to 2.5 s. Regarding the healthy motor, one can observe the smooth transitions of the harmonic components from 0 to 0.5 s, as well as the stabilisation of those trajectories in the steady state.

Regarding the faulty motor's stator current spectrogram depicted in Fig. 7 (adjacent case), the V-shaped pattern is identified which is a pattern indicative as a symptom of broken rotor bars [4–7, 16]. Also, the intensity of the harmonic trajectories' spectral content during the start-up transient is obviously more intense compared to the healthy motor.

Additionally, Fig. 8 shows the spectrogram of the stator current for one of the cases of two non-adjacent broken bars within half-pole pitch. The spectrogram is rich in fault-related harmonics, as one can see in the time interval from 0 to 1.5 s and the V-shape pattern is present here as well.

Nevertheless, the current spectrogram is providing sufficient information to identify this type of fault, but not adequate enough to detect the fault location and severity.

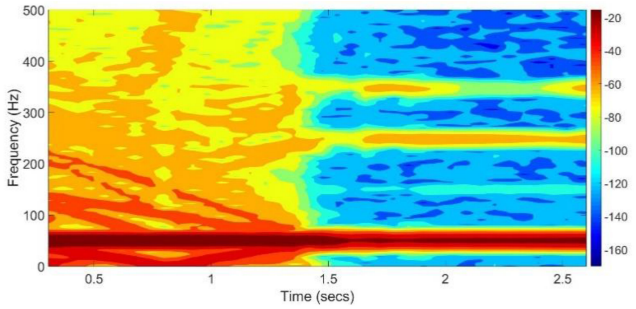

Fig. 8 *Stator current STFT spectrogram of motor with broken bars in non-adjacent positions (Case III)*

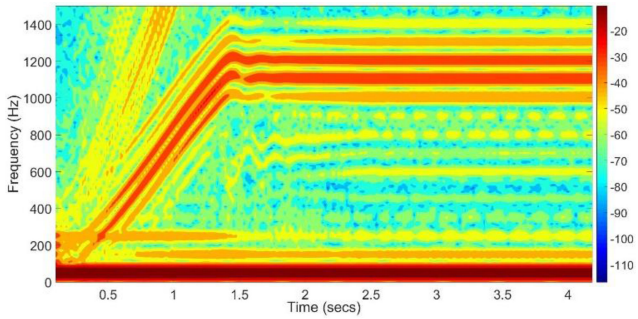

Fig. 9 *Flux sensor voltage STFT spectrogram of healthy motor*

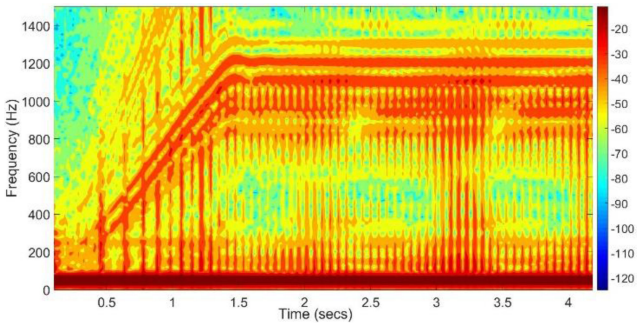

Fig. 10 *Flux sensor voltage STFT spectrogram of motor with adjacent broken bars (Case II)*

In order to evaluate those, stray flux monitoring and analysis will be implemented. Fig. 9 illustrates the flux sensor's voltage during transient (0–2.5 s) and steady state (2.5–4 s) and for the frequency range of 0–1.2 kHz.

It should be noted that in machines like the one under study, the frequency range for harmonics identification should be up to 2.5 kHz in order to discriminate high-order harmonics [8, 10, 17] and principal slot harmonics [18]. However, the focus of this work will be on the behaviour of the radial flux harmonics [15, 19], which belong to the frequency range depicted in the following spectrograms.

The flux sensor voltage spectrogram of the motor with two adjacent broken bars is providing information in some specific time windows, in terms of frequency bands, with varying spectral energy density (Fig. 10). These bands appear on the spectrogram periodically and this is due to the periodicity according to which the broken bar crosses the neutral zones of the rotating magnetic field. This periodical effect becomes more tangible and clearly visible in the following cases, where the distance between the broken bars allows the fault to make its presence in more time-frames. The fact that these frequency zones appear as one in terms of periodicity, is due to the fact that the broken bars are adjacent, hence two adjacent broken bars are identified as one bar with larger breakage.

In the non-adjacent case of Fig. 11, it is clear that some harmonic trajectories provide information about the broken bar fault and its periodicity, while their presence and behaviour is more intense compared to the healthy case in Fig. 9 and the case of

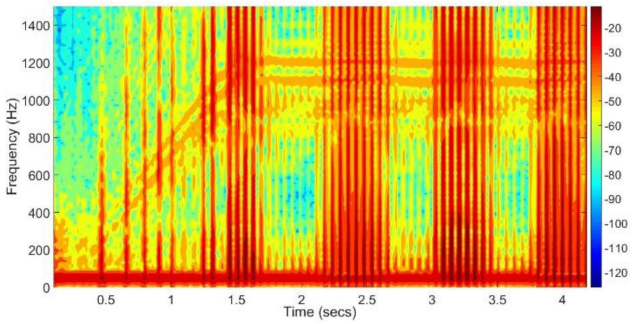

Fig. 11 *Flux sensor voltage STFT spectrogram of motor with non-adjacent broken bars (Case III)*

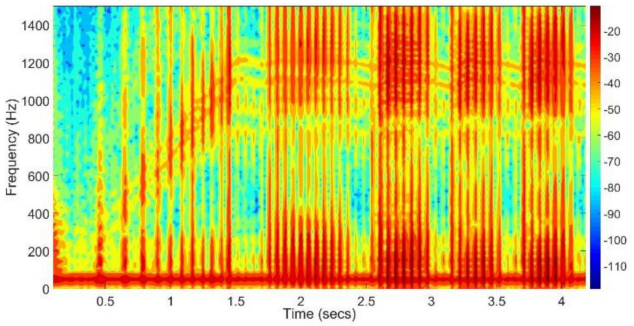

Fig. 12 *Flux sensor voltage STFT spectrogram of motor with non-adjacent broken bars (Case IV)*

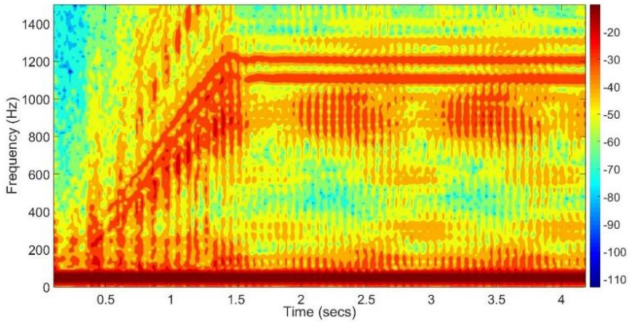

Fig. 13 *Flux sensor voltage STFT spectrogram of motor with non-adjacent broken bars (Case V)*

adjacent broken bars in Fig. 10. Also, the periodicity with which these cross-terms appear is now varying, and this variance is corresponding to the increased angular position of the broken bar. Similar is the case of the broken bars within one pole pitch (Case IV), with the difference that the phenomenon makes its presence earlier in the start-up transient with more high energy cross-terms (Fig. 12). Another interesting observation in Figs. 11 and 12 is the oscillation of trajectories around these cross-terms for the frequency band of 0.9–1.2 kHz, especially during the steady-state regime.

Finally, in the Case V which accounts for broken bars in positions 1 and 23 (within two pole's pitch), the diagnostic image changes. The cross-terms observed in the previous cases are appearing obscured and the image of symptoms is very similar to Case II (adjacent broken bars). This is probably because the effect of broken bars is masked with regard to the broken bars distance increase. Apparently, the broken bar fault in such position is giving wrong indications on the spectrogram; thus leading to possible misdiagnosis since this specific fault severity appears to be low (see Fig. 13).

4 Conclusion and future work

This paper deals with a new approach to detect non-adjacent broken rotor bars in induction motors at steady state via monitoring the external flux. The results imply that a time-frequency approach

is worth not only when focusing on the behaviour of the monitored signals during the start-up transient, but should also search in the steady state for patterns indicative for faults. The stator current spectrogram was used to identify the type of fault and the stray flux for evaluating the fault severity. Future work on this study intends to proceed with post-processing and image processing for identification and specific modelling of the areas where the fault makes its presence, as well as a mathematical formulation of these.

5 Acknowledgments

This work was supported by the Research Centre for Mobility and Transport and Coventry University, UK.

6 References

[1] Sobczyk, T.J., Maciolek, W.: 'Is the (1–2 s)f0 in stator currents sufficient for detection of rotor cage faults?'. IEEE Int. Symp. on Diagnostics for Electric Machines, Power Electronics and Drives (SDEMPED), 2005

[2] Sizov, G.Y., Sayed-Ahmed, A., Yeh, C.-C*., et al.*: 'Analysis and diagnostics of adjacent and nonadjacent broken-rotor-bar faults in squirrel-cage induction machines', *IEEE Trans. Ind. Electron.*, 2009, **56**, (11), pp. 4627–4641

[3] Riera-Guasp, M., Pons-Llinares, J., Vedreno-Sanots, F*., et al.*: ' Evaluation of the amplitudes of high-order fault related components in double bar faults'. IEEE SDEMPED, 2011

[4] Zanardelli, W.G., Strangas, E.G., Aviyente, S.: 'Intermittent fault identification for permanent magnet AC drives based on the short-time Fourier transform'. IEEE SDEMPED, 2005

[5] Antonino-Daviu, J.A., Gyftakis, K.N., Garcia-Hernandez, R*., et al.*: 'Comparative influence of adjacent and non-adjacent broken rotor bars on the induction motor diagnosis through MCSA and ZSC methods'. IEEE IECON, 2015

[6] Lopez-Ramirez, M., Romero-Troncoso, R.J., Morinigo-Sotelo, D*., et al.*: 'Detection and diagnosis of lubrication and faults in bearing on induction motors through STFT'. IEEE 2016 Int. Conf. on Electronics, Communications and Computers (CONIELECOMP), 2016

[7] Georgoulas, G., Climente-Alarcon, V., Dritsas, L*., et al.*: 'Start-up analysis methods for the diagnosis of rotor asymmetries in induction motors – seeing is believing'. 24th Mediterranean Conf. on Control and Automation (MED), 2016

[8] Wang, C., Zhou, Z., Unsworth, P.J*., et al.*: 'Sensorless speed measurement of induction machines using short time Fourier transformation'. IEEE SPEEDAM, 2008

[9] Sizov, G.Y.: ' Analysis, Modeling, and Diagnostics of Adjacent and Nonadjacent Broken Rotor Bars in Squirrel-Cage Induction Machines'. B.S.E.E. Thesis, Marquette University, 2007

[10] Gyftakis, K.N., Antonino-Daviu, J.A., Marques Cardoso, A.J.: 'A reliable indicator to detect non-adjacent broken rotor bars severity in induction motors'. IEEE Int. Conf. on Electrical Machines (ICEM), 2016

[11] Cupertino, F., de Vanna, E., Salvatore, L*., et al.*: 'Comparison of spectral estimation techniques applied to induction motor broken bars detection'. IEEE SDEMPED, 2003

[12] Kia, S.H., Henao, H., Capolino, G.-A*., et al.*: 'Induction machine broken bars fault detection using stray flux after supply disconnection'. IEEE IECON, 2006

[13] Aimer, A.F., Hamida Boudinar, A., Benouzza, N*., et al.*: 'Simulation and experimental study of induction motor broken rotor bars fault diagnosis using stator current spectrogram'. IEEE Int. Conf. on Control, Engineering and Information Technology (CEIT), 2015

[14] Gröchenig, K.: '*Foundations of time-frequency analysis*' (Springer Science & Business Media, New York, 2013)

[15] Georgoulas, G., Climente-Alarcon, V., Antonino-Daviu, J.A*., et al.*: 'A multi-label classification approach for the detection of broken bars and mixed eccentricity faults using the start-up transient'. IEEE 14th Int. Conf. on Industrial Informatics (INDIN), 2016

[16] Sobczyk, T.J., Maciolek, W.: 'Diagnostics of rotor-cage faults supported by effects due to higher mmf harmonics'. IEEE Bologna Power Tech Conf. Proc., 2003

[17] Cabal-Yepez, E., Garcia-Ramirez, A.G., Romero-Troncoso, R.J*., et al.*: 'Reconfigurable monitoring system for time-frequency analysis on industrial equipment through STFT and DWT', *IEEE Trans. Ind. Inf.*, 2013, **9**, (2), pp. 760–771

[18] Wang, C., Zhou, Z., Unsworth, P.J*., et al.*: 'Current space vector amplitude fluctuation based sensorless speed measurement of induction machines using short time Fourier transformation'. 34th Annual Conf. of IEEE Industrial Electronics, 2008

[19] Menacer, A., Champenois, G., Nait Said, M.S*., et al.*: 'Rotor failures diagnosis of squirrel cage induction motors with different supplying sources', *J. Electr. Eng. Technol.*, 2009, **4**, (2), pp. 219–228